Received 22 December 2023; revised 12 February 2024; accepted 16 February 2024. Date of publication 19 February 2024; date of current version 24 September 2024.

Digital Object Identifier 10.1109/OJAP.2024.3367664

Analysis and Design of Planar Surface Wave Lenses and Application to Leaky-Wave Antennas

MAKSIM V. KUZNETCOV[1] (Member, IEEE), DAVIDE COMITE[2] (Senior Member, IEEE), SYMON K. PODILCHAK[1] (Member, IEEE), ALOIS P. FREUNDORFER[3,4] (Life Senior Member, IEEE), AND YAHIA M. M. ANTAR[3,4] (Life Fellow, IEEE)

[1]Institute of Imaging, Data and Communications, The University of Edinburgh, EH9 3JW Edinburgh, U.K.

[2]Department of Information Engineering, Electronics and Telecommunications, "Sapienza" University of Rome, 00184 Rome, Italy

[3]Department of Electrical and Computer Engineering, The Royal Military College of Canada, Kingston, ON K7K 7B4, Canada

[4]Department of Electrical and Computer Engineering, Queen's University, Kingston, ON K7L 3N6, Canada

CORRESPONDING AUTHOR: D. COMITE (e-mail: davide.comite@uniroma1.it)

The work was supported by The Royal Military College of Canada, Queen's University, and The University of Edinburgh.

ABSTRACT Planar metasurface lens structures based on microstrip technology, optimized to control the propagation of surface waves (SWs), are presented. Two different lenses are studied, i.e., a converging or plane-wave-like lens and a diverging lens. Near-field simulations and measurements are reported to demonstrate the guiding features of the designed lenses, which have also been proposed as a feeding system for planar leaky-wave antennas (LWAs). Far-field results show improvements in terms of reduced cross polarization and sidelobe level as well as increased realized gain when compared without these SW lenses. The proposed structures are also simple to manufacture and are employed herein to control SW fields generated by a TM_0 surface-wave launcher (SWL) integrated in the ground plane of the developed prototype demonstrators. Some applications include high-gain radar and remote sensing satellite antennas as well as microwave and millimeter-wave communication systems.

INDEX TERMS Metasurfaces, leaky-wave antennas, surface waves, feeding systems.

I. INTRODUCTION

METASURFACES and metamaterials are useful and versatile for designing new devices and antennas [1], [2], [3]. These structures typically have printed, sub-wavelengths inclusions and can be exploited in the design process to enable new techniques to control the propagation of guided waves and surface waves (SWs); this is desirable for antenna size reduction as well as improved impedance matching and lower cross-polarization levels, for example. One of the earliest investigations into metasurfaces was reported in [4], where theoretical considerations of artificially soft and hard surfaces were described. In particular, the characteristics of different corrugation loading (also defined as *hard*) and unloaded (*soft*) elements were studied showing field control.

Efficient and modern antennas using metasurfaces require proper design of the surface profile, which is generally based on modeling approaches and suitable approximations. For example, an antenna system based on the use metasurfaces was proposed in [5]. In that work, a loop-wire unit-cell printed on a dielectric substrate was presented, and modulation techniques were exploited to simultaneously support TM and TE SW modes. By tailoring the geometrical parameters of the loop-wire structure, optimum control of the SW phase propagation constants was achieved, and this supported the excitation of both a TM and a TE SW mode for radiation [5]. A directivity of 25.6 dBi and 20.7 dBi was achieved, respectively, however, the bandwidth for this structure was limited due to the overlapping of the TM and TE SW modes, which occurred over a narrow frequency range.

Another popular approach for antenna design leverages on the use of high-impedance surfaces (HIS) [6], [7]. Typically, HISs can act as artificial magnetic conductors (AMC) or perfect magnetic conductors (PMC). Cross-shaped elements,

meandered cells, and compact patch structures have all been reported [6], [7], [8], [9]. In [7] for example, the bandwidth and radiation characteristics of a monopole were enhanced by introducing a square-shaped metamaterial on an additional ground plane under the printed monopole antenna. The reported bandwidth was 55.6% with a maximum gain of 10.2 dBi. This offered gain improvement of about 7 dBi, with respect to a more standard monopole antenna.

Metasurfaces have also been proposed as reflectors in the design of directive antennas and for reduced radar cross-section. In [10], a dual-band metasurface-based reflector was presented, which operated from 18.2 to 24.6 GHz and 40.6 to 56.4 GHz. The printed unit cells of the reflector consisted of rhombus-shaped patches having annular configurations. Reconfigurable structures have also been of interest, as in [11], where a low-profile switchable metasurface antenna was presented. The design operated from 4.2 to 5.5 GHz and consisted of a ring-shaped pixel structure, equipped with 16 pin diodes and this allowed for controlling the polarization state of the antenna. Structures based on Huygen's surfaces have also been examined [12]. They are typically based on periodic strips or some reactive surface sheets, and this enables versatile control of the propagating SWs. For example, in [13], a design methodology was demonstrated for development of a beam-refracting surface and a Gaussian-to-Bessel beam transformer.

The concept of lensing [14], [15], at microwave frequencies has also been reported for antenna feeding networks. Basically, at microwave frequencies, dielectric lenses can be designed to control and shape free-space waves from a central source. For instance in [15] and [16] lenses were employed to achieve increased gain values from microstrip patch elements for an antenna array configuration. Similarly, volumetric lens antenna structures for wave control [17] have also been realized by the periodic loading of metallic elements within a host dielectric. This can be considered a 3-D artificial material, with an effective dielectric constant that can be slightly larger than that of the unloaded or free-space medium.

Following these earlier techniques to control SWs using metasurfaces and microwave lensing, and in an effort to ease fabrication in such a volumetric 3-D lens systems [17], new planar metallic surface wave (SW) lenses are investigated in Section II. In particular, by the addition of a periodic configuration of microstrip lines (of width W) placed on top of a grounded dielectric slab (GDS), which supports planar SWs generated by a TM SW source, phase constant values larger than that of the surrounding dielectric medium can be engineered. Moreover, as shown in the following, the designed converging and diverging SW lenses are optimized to feed planar leaky-wave antennas (LWAs) with improved gain and reduced sidelobe levels with respect to more conventional implementations (i.e., without the lens). Findings are supported by near-field studies of the designed lenses as well as simulations and measurements of the examined LWAs in Sections III and IV, respectively. A summary of the work is provided in Section V to conclude the paper.

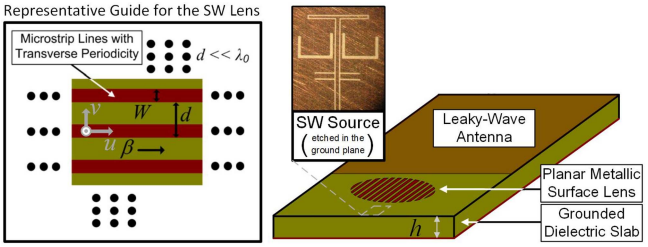

FIGURE 1. Planar metallic surface lens for control of bound TM SWs. The medium defining the 2-D lens structure is modeled as a simple grid or (non-radiating) array of printed microstrip lines; i.e., a transverse periodic microstrip guide (TPMG) having width W and spatial periodicity d in the transverse v-direction (see left), which is sub-wavelength. The SW source and leaky wave (LW) part of the antenna structure (see right) is also shown.

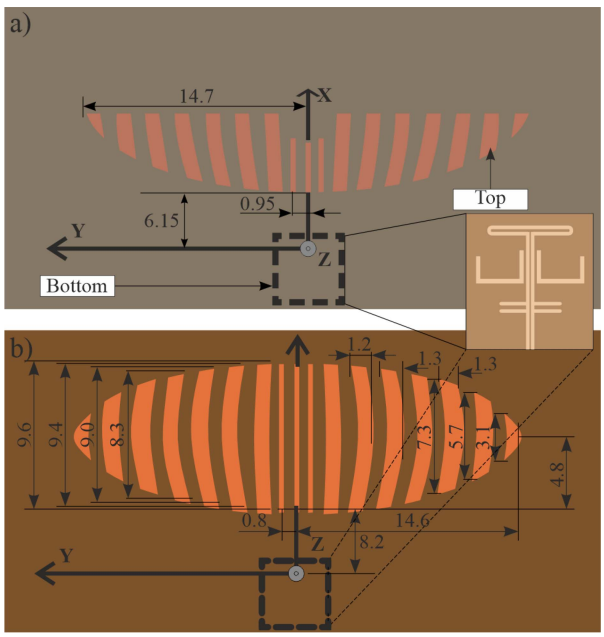

FIGURE 2. Designed and fabricated SW lens structures with their dimensions in mm: a) plane-wave (or converging) lens, b) diverging lens. The planar structures are printed on top of the GDS while the SWL feed is positioned in the ground plane (or in the bottom side of the PCB, see Fig. 1).

II. THEORETICAL CONSIDERATIONS

This section outlines the planar lensing technique to control SW fields. For example, by the addition of a sub-wavelength metallic-strip grating (MSG) configuration, placed on top of the guiding surface and parallel to the direction of SW propagation β (see Fig. 1), an effective dielectric constant can be achieved refracting and controlling SW fields transmitted from a central source.

Two printed surface lenses will be investigated as shown in Fig. 2 which have been optimized using a commercial full-wave solver. It will also be shown in the following that these lenses enforce a divergence of the SWs and the transformation from a cylindrical wave into a bound plane wave when considering transmission from a central SW

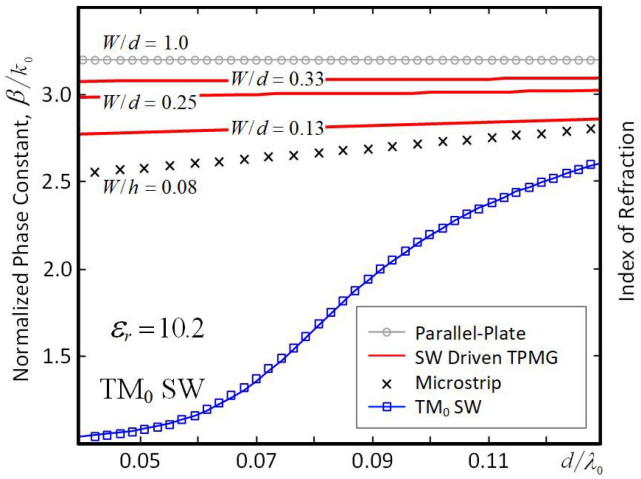

FIGURE 3. Numerically determined phase constant values, $\hat{\beta} = (\beta/k_0)$, compared to the TM_0 SW mode as well as the fundamental parallel-plate mode of the host GDS (markers). Results are also compared to full-wave simulations for the TPMG (continuous lines). In the operating frequency range of the SW lens the transverse periodicity, d, is sub-wavelength; i.e., $d << \lambda_0$.

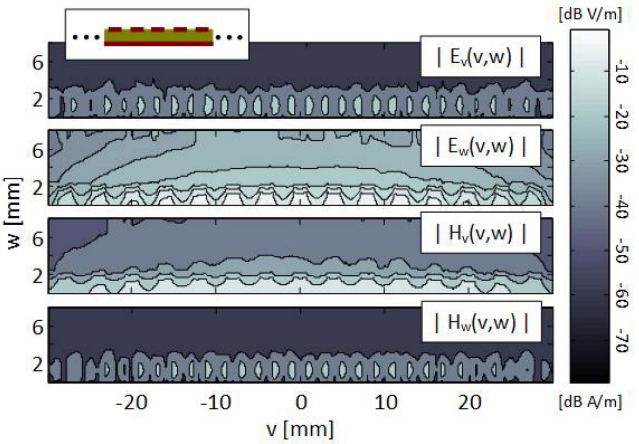

FIGURE 4. Simulated field distribution for the TPMG (see Fig. 1) due to an incident TM SW at 24 GHz considering a substrate height of h of 1.27 mm and $\varepsilon_r = 10.2$. Values normalized to the observed maximum for the excited fields within the guide and with E_w and H_v respectively dominant defining a TM field configuration.

source. Likewise, in a receiver configuration, this defines a SW focusing effect or the convergence from a bound plane-wave to a source positioned at the origin.

A. PLANAR SW FEEDING

To feed these SW lens designs, a directive Yagi-Uda type surface-wave launcher (SWL) is employed as the planar source, and with a 50-Ω co-planar feedline extending to the edge of the substrate (see [18, Fig. 3] for the relevant dimensions of the SWL). To ensure efficient coupling into the dominant TM_0 SW mode of the GDS, with values of 90%, an electrically thick substrate of height h (= 1.27 mm) with a relatively high dielectric constant value (ε_r = 10.2) was used as the host guiding structure [19]. It is well known that these SWLs can generate a cylindrical TM SW field distribution, and this is useful for feeding planar antenna structures for operation from about 18 to 26 GHz.

B. LENS FIELD PROFILE AND SYNTHESIS

We will now focus our attention on defining the field quantities that can be generated within the lens region due to an incident TM SW from the SWL. In Fig. 1(left) the concept is illustrated: the SW lens structure is represented by a longitudinal arrangement of printed and closely packed microstrip lines and with a common periodicity d (i.e., a TPMG).

Figure 3 shows the normalized phase constant values for three TPMGs that can be adapted for these SW lenses, i.e., $W/d = 0.13$, 0.25, and 0.33. It is also important to note that the transverse periodicity d for these structures is sub-wavelength. It can also be observed that normalized phase constant values, i.e., $\beta/k_0 = \hat{\beta}$ for these TPMGs, are greater when compared to that of the TM_0 SW mode of the GDS (or the unloaded structure), similarly for the fundamental mode of quasi-TEM microstrip. These results suggest that the TM phase constant can be tailored and enhanced when compared to the unloaded GDS, and when introducing the TPMG after the SW source. As also observed in Fig. 3, the refractive index of the TPMG, or lens region, approaches $\sqrt{\varepsilon_r}$ (= 3.194) which corresponds to the conventional TM parallel-plate waveguide (PPW) mode. This is because the fields are mostly contained within the dielectric (see Fig. 4) for the partially closed TPMG, suggesting that the TPMG behaves as a quasi-uniform parallel-plate guide. A TM SW-like field distribution can be supported at microwave and millimeter-wave frequencies defining the metasurface microstrip-based waveguide.

For synthesis procedures the planar lens can be characterized as an effective medium. In particular, at the operating frequency of the SWL, the guided TM_0 SW mode can be represented by an effective refractive index, $\hat{\beta} = n_1 = 2.1$ at about 0.09 d/λ_0 (see Fig. 3, which is approximately 23 GHz and chosen as our central design frequency). Here we define n_1 as the refractive index of the GDS region surrounding the lens (see Fig. 1). Furthermore, since the vertical E_z field component of the TM SW is well matched to the fields of the TPMG, SWs from the SWL can couple power into the lens region with reduced reflections [19] as the TPMG and GDS regions have similar phase constant values.

A TM field configuration is generated within the lens region and can be modeled using a second index of refraction: $n_2 \approx 3.1$ considering $W/d \approx 3$. More importantly, control of the incident SW field occurs due to refraction, i.e., the effective index for the lens region is greater than the surrounding dielectric medium (i.e., $n_2 > n_1$). This is because the phase constant or refractive index for the TPMG, within the lens region, is greater than the TM_0 SW mode. This realized refractive index for the lens can be defined as $n = n_2/n_1 \approx 3.1/2.1 = 1.476$ and this value can be used for further lens synthesis using the ray tracing technique [20].

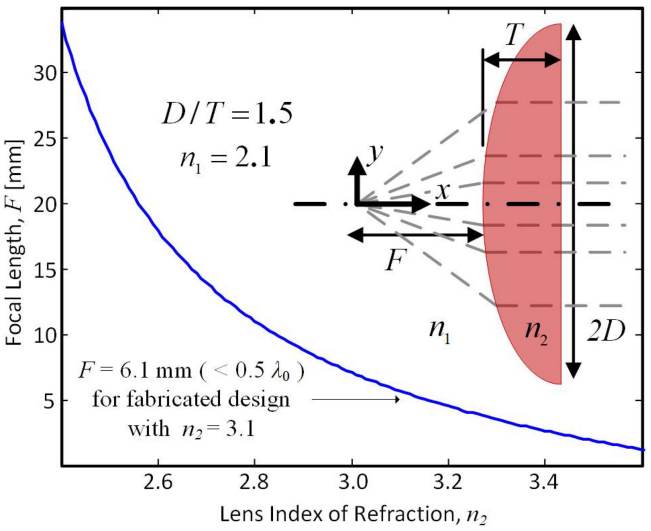

FIGURE 5. Calculations of the focal length, or required SW source position, for the plane-wave lens, by [14] $F = D^2 + T^2(1 - n^2)/2T(n - 1)$.

For instance, focal length and lens dimensions where initially calculated using n_2 for the TPMG, see Fig. 5 for the plane-wave lens. The reciprocal process is also possible where a bound plane wave culminates into a single focal point F (i.e., to a receiver element) at the origin.

Further improvements in accuracy, in terms of the exact index of refraction for the SW lenses, may be achieved by further characterization of the TPMG for each strip width and periodicity while also including curvature effects. However, for a first order model, this approximation for the TPMG and lens region may be suitable for an initial synthesis procedure of the SW lens, its design and implementation. Following these results, further optimization of the grating lenses was carried out in a commercial full-wave solver to ensure reduced reflection coefficient values at the input of the SWL (which were ≤ -10 dB from about 20 GHz to 26 GHz, see [19, Fig. 6.12]), while also, maintaining the desired lens functionality.

Overall, the planar metallic lens design process can be summarized as follows:

1) The first step involves characterizing the SW guide structure for the lens. As described above this involves defining a representative medium for the lens region and determining an approximate value for the normalized phase constant $\hat{\beta}$ or the effective refractive index n_2, which should be higher than the GDS region n_1.
2) Identify the normalized index of the refraction for the SW lens and use standard lens ray-tracing techniques [20] to determine an initial lens size and dimension, with respect to the SWL source positioned at the origin.
3) Further optimize the lens shape for the desired functionality (diverging or converging), also in conjunction with the SWL using full-wave simulators.

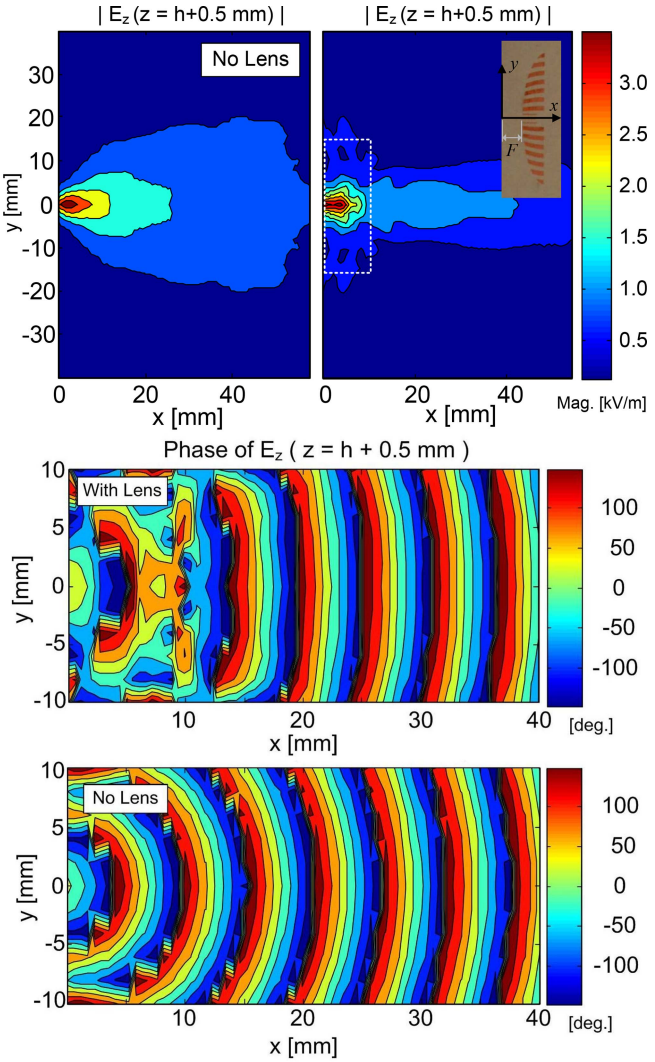

FIGURE 6. Simulated TM fields generated on the guiding surface with and without the SW lens. A bound and guided plane wavefront can be observed by introducing the SW lens.

By following Fig. 5 for the plane-wave (or converging) SW lens and the above design procedure, the thickness of the lens T can be increased to realize a diverging SW lens. In our work we initially optimized the plane-wave lens, and then approximately doubled the value T (see Fig. 5, inset) for the diverging SW lens.

C. FULL-WAVE SIMULATIONS OF THE SW LENS

The planar metallic metasurface lenses were designed to achieve controlled SW propagation along the employed GDS and in conjunction with the SW source. Specifically, by the addition of these planar lenses, the excited TM SWs from the SWL were controlled and refracted by the metasurface TPMG lens region. In particular, the cylindrical wave front excited by the SW source at the origin is altered by the planar lens. The resultant field distribution on the GDS generated by the SW source and lenses are shown in Fig. 6 at 23 GHz. It can be seen that a bound plane-wave is generated by

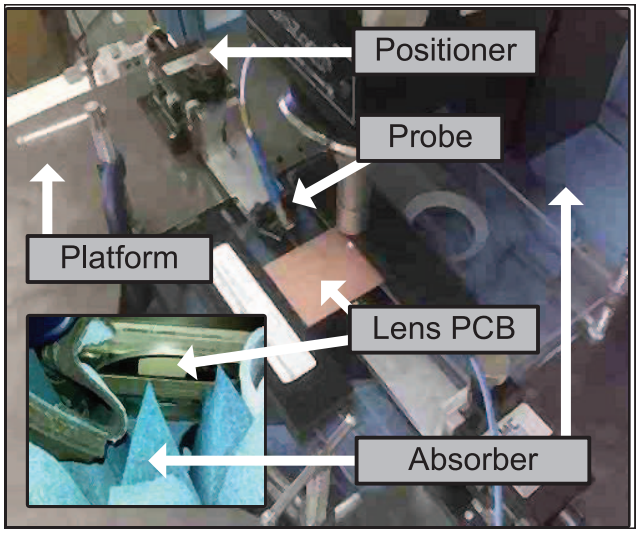

FIGURE 7. Near-field measurement setup used to sample the TM SWs for the proposed metasurface lenses. The platform with the integrated circuit probe is shown as well as the microwave absorber, which was positioned below and at the perimeter of the lens PCB test structures to minimize edge reflections. The inset also shows the underside of the setup.

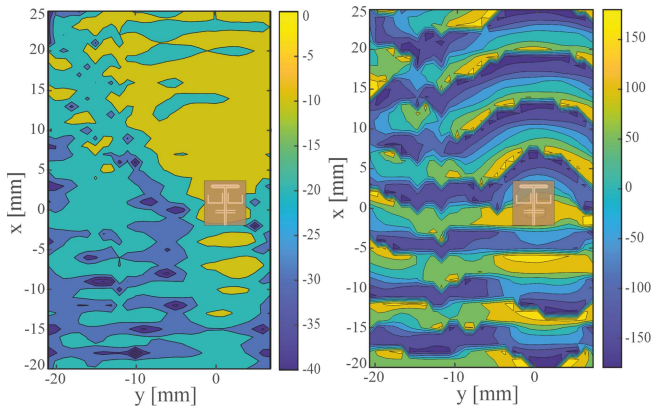

FIGURE 8. Measured magnitude and phase response above the air-dielectric interface generated by the directive SWL positioned at the origin (an image of the SWL is also shown defining its relative position). As can be observed the TM field is directed in the forward *x*-direction and a cylindrical wave profile is achieved as expected.

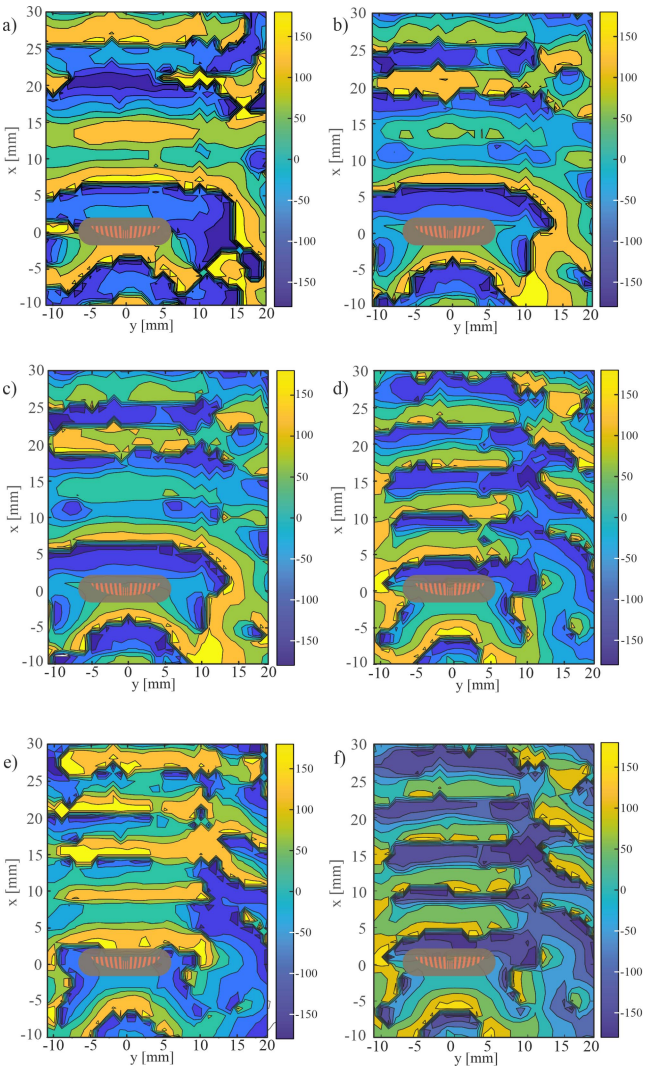

FIGURE 9. Measured phase response of the plane-wave lens at a) 20.5 GHz, b) 20.8 GHz, c) 20.85 GHz, d) 21.55 GHz, e) 21.6 GHz, f) 21.8 GHz. As can be observed in the phase profile, a general uniform phase front is shown in the forward direction. Also, for the measurement setup, the location of the lens is illustrated.

the addition of the lens and this is observed both in the magnitude and phase. Similar results were observed for the diverging lens (see [19, Fig. 6.16], all results not shown for brevity) when compared to the no lens case, albeit the magnitude of the TM fields were further dispersed along the air-dielectric interface. These findings are consistent with the model in Fig. 5, given that the distance F for the optimized plane-wave lens was about 6 mm and considering the refractive index for the metasurface lens region n_2 (that for the TPMG is about 3).

III. METASURFACE LENS: EXPERIMENTS AND DISCUSSIONS

The optimized and manufactured prototype SW lenses, considering both a diverging and a plane-wave lens as reported in Fig. 2, were measured in the near-field about 0.5 mm above the air-dielectric interface. The measurement setup, see Fig. 7, was designed to sample the TM field values generated by the SWLs and lens configurations. Comparisons of the measurements without and with the lenses are reported in Figs. 8 to 10. Basically, test circuits were manufactured for near-field measurements, which only had the lenses and the SWL feeds.

The co-planar waveguide feedlines for the SWLs were connected to a standard vector network analyzer using integrated circuit (IC) probes (PICO model 40A-GSG-150-P) and *x*-*y*-*z* positioners. A retro-fitted IC probing station was also used to sample the field profile underneath the PCB (see Fig. 7). This is because the test structures were measured with the SWLs on top (or ground plane on top) and with the lenses below. Microwave absorbering materials were also placed at the edge of the PCBs to minimize any edge reflections. Also, to ensure a suitable air-dielectric interface

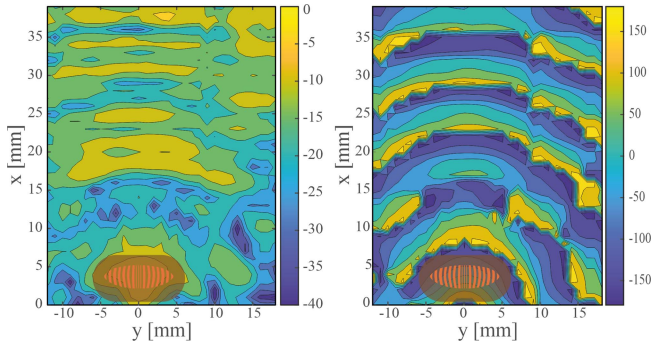

FIGURE 10. Measured magnitude (left) and phase (right) of the TM field generated by a diverging lens and SWL at 21.1 GHz. The spreading of the wave can be clearly observed when compared to Fig. 8 as well as the phase response. The location of the lens is also illustrated.

for SW excitation and propagation along the slab, a hole was cut in the probing station platform (see Fig. 7 inset). Absorbers were also used to isolate the metallic probing station from the SW lenses and SWLs under test.

The field generated by the directive SWL in the absence of the proposed lenses is reported in Fig. 8. A slight offset of the aperture was sampled to fully observe the front and back field profile of the SWL. As shown, the majority of the power is directed in the forward region with field values about 20 dB higher in front of the launcher than behind. It is also important to note that the phase profile demonstrates a conical shape, from about $y \in [0, 25]$ mm. This is expected since the SWL (with no lens) generates a cyclindrical-like field profile in the forward x-direction [19].

The measured plane-wave SW lens response, considering different frequencies from 20.5 GHz to 21.8 GHz, is reported in Fig. 9. At frequencies equal to 20.9 GHz, 20.85 GHz, and 21.8 GHz, the uniform phase front correction is clearly visible, i.e., the fields originating from the SWL are transformed from a cylindrical wavefront to a quasi-planar wavefront after the lens. Some samples show a slightly indistinguishable result, but improvements are clearly visible further away from the SWL and a continued planar wavefront is still generally observed. There is also a noticeable disruption to the wavefront for $y > 15$ mm, which is related to reduced signal power, as the majority of the SW field strength is directed in the forward direction and contained within $x \in$ [-10, 10] mm, and this is consistent with Fig. 6.

The magnitude and phase response of the SWL and diverging lens are reported in Fig. 10. Results show that the TM field is dispersed across the manufactured PCB and with relatively constant field strengths. For example, values are about -20 dB (or above) mostly across the air-dielectric aperture in the forward direction. Basically it can be observed that the SW fields were guided and spread across the PCB showing a diverging SW field profile, i.e., a high concentration of the field can be seen $x, y \in$ [10 to 35, $\pm$5] mm. Conversely, for the SWL alone, TM fields values decrease to below -15 dB for $y > -15$ mm. For

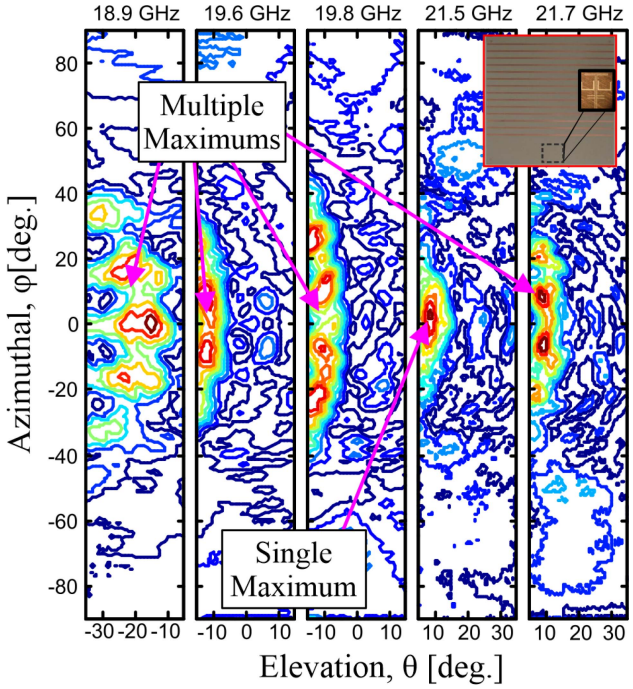

FIGURE 11. Measured 2-D beam patterns normalized and shown in linear units for the MSG-based LWA and directive SWL feed (see inset). Single or multi-beam patterns are observed as a function of frequency.

this measurement setup the position of the SWL was at the origin.

These near-field measurements demonstrate that the planar lens shown in Fig. 2 can properly shape the fields excited by the SWL. By the addition of printed microstrip lines, placed on top of the guiding surface and parallel to the direction of SW propagation, an effective dielectric constant can be achieved refracting and controlling SWs. Therefore these microstrip-based, sub-wavelength designs can act as metasurface lenses to control and direct cylindrical SW fields generated by the SWLs. In particular, the TM field profiles of two metallic surface lenses have been measured at the air-dielectric interface, demonstrating the transformation from a cylindrical wave into a bound plane-wave and the divergence of TM SW fields.

IV. LEAKY-WAVE ANTENNA DESIGN

By utilizing SWs on a GDS and properly designing MSGs for radiation, leaky waves (LWs) can be excited by the $n = -1$ spatial harmonic; this realizes the transformation from a bound SW mode to a radiated mode [19], [21], [22]. In this section the proposed SW lenses are exploited and demonstrated to shape the phase of the TM SW fields, and this is used to feed planar LWAs.

A. 1-D LWA AND INTEGRATION OF A PLANE-WAVE LENS

We first analyze here the radiation features of a conventional 1-D periodic microstrip-based LWA (MSG periodicity of 6.3 mm and strip width of 1.25 mm), reported within the

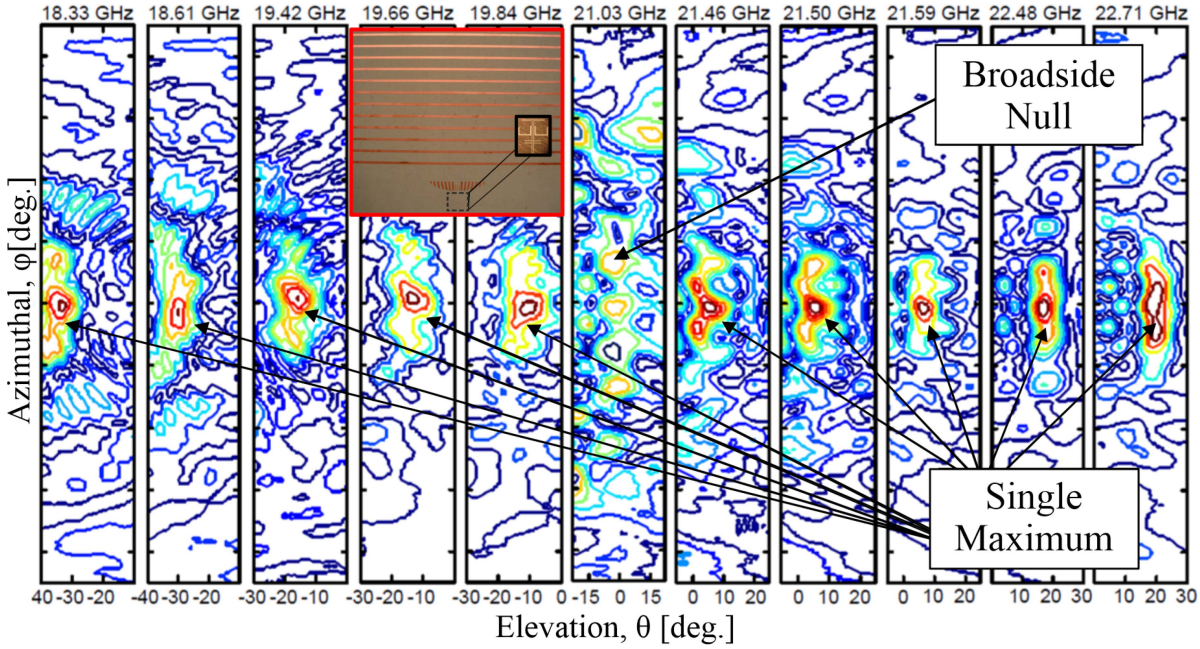

FIGURE 12. Measured 2-D far-field beam patterns for the LWA in Fig. 13. A single pencil beam is shown suggesting lens functionality. One-sided, backward [forward] beam patterns are observed for f < 20 GHz [f > 21 GHz] with a broadside null from 20.0 to 21.3 GHz suggesting a LW stop band.

inset in Fig. 11 and considering a directive SWL as the antenna feeder. As shown in Fig. 8, the wavefront of the SW generated by the SWL alone produces a non-uniform phase profile, this reduces the radiation performance (i.e., the peak directivity and pattern shape, for example) of such a conventional LWA structure.

The radiation performance of this LWA (with no lens included) is reported in Fig. 11; the measured profile shows the 2-D far-field beam patterns scanning as a function of frequency. High sidelobe levels are observed and, for example, at 19.8 GHz a multiple-beam pattern is shown; this is generally unwanted as LWAs are typically designed for supporting a directive single-beam pattern, with reduced sidelobe levels. For this LWA configuration, the cylindrical TM SW couples to the linear MSG developing periodic current distributions, and this generates a standing wave pattern on the finite grating realizing the noted multi-beam pattern in the far-field. Maximum and minima of the corresponding antenna gain are observed.

To improve the radiation characteristics of such a LWA, the plane-wave lens outlined in Fig. 2 was further integrated with the antenna structure. Basically, the plane-wave profile enforced by the metasurface lens allows for a more uniform distribution of the TM_0 SW mode. In particular, the MSG for radiation perturbs the SW across the aperture, generating LW radiation with a more directive single-beam pattern, which scans as a function of frequency in the far-field. The dispersion profile for these types of MSG-based LWAs, defined by the LW phase and attenuation constant, β and α, respectively, have been further investigated in [19], [23], [24].

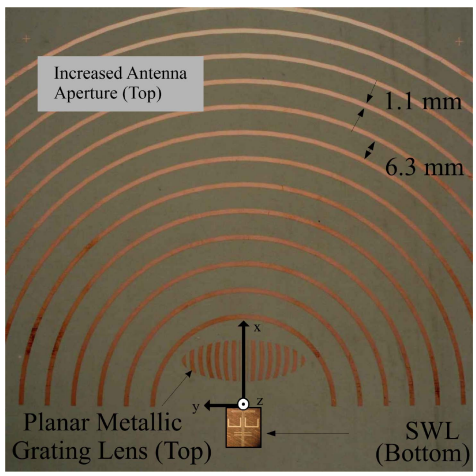

FIGURE 13. Manufactured planar LWA to demonstrate diverging lens functionality by the addition of the planar metallic SW lens on top of the GDS. The added MSG, for radiation, has a periodicity *d* of 6.3 mm and the strip width *w* is 1.1 mm.

When comparing Figs. 11 and 12, improved radiation performances are demonstrated. In particular, the 2-D far-field plots show a single-beam maximum that scans as a function of frequency. This is mainly a result of uniform current distributions being generated on the MSG when the plane-wave SW lens is added. With such an enlarged effective aperture, when compared to the same structure with no lens [22], directive pencil beam patterns are generated in the far-field.

B. HALF-ANNULAR LWA WITH A DIVERGING LENS

Half-annular LWAs, as those proposed in [21], [22], [23], are considered in this section. It is constituted by one half

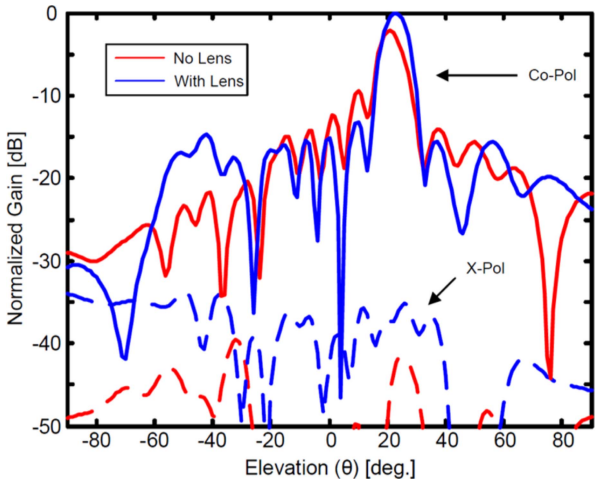

FIGURE 14. Measured half-annular LWA with and without the plane-wave lens. The improvement is almost around 3 dB$_i$ and with sidelobe level reduction for the first lobe. To ensure a common aperture size, the LWA with a diffracting lens and 13 strips was also compared to a more conventional design with 15 strips.

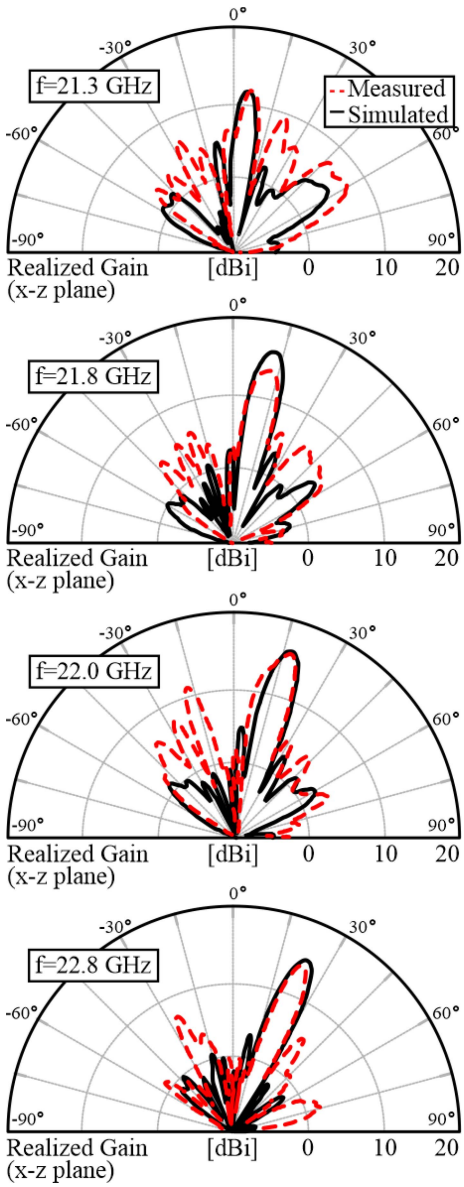

FIGURE 15. Comparison of the measured and simulated beam patterns for the LWA in Fig. 13. Gain values are greater than 14 dB$_i$ from 21.8 GHz to 22.8 GHz.

of a more conventional bull-eye LWA (see Fig. 13), whose strip arrangement is exactly annular, and therefore, the phase front produced by the TM_0 SWL, as shown in Fig. 8, is not ideally matched to the entire half-annular MSG profile. However, by using a diverging metasurface lens, increased gain values can be observed for the same LWA defined by a half-annular MSG (see Figs. 14 and 15). This is because the SWL alone directs TM SW fields within a confined region and thus not fully illuminating the aperture.

Figure 14 reports a comparison of the normalized beam pattern radiated by the half-annular LWA with and without the lens. It should be noted that the physical aperture sizes are not exactly the same. This is because the number of LW radiating strips was reduced from 15 to 13 to accommodate the position of the lens near the origin. This was needed to maintain a common PCB size for the measurement setup in the anechoic chamber and when placing the AUT on the angular positioner. This inadvertently resulted in a decrease of the physical aperture size due to the presence of the lens. Regardless, the realized gain improved by almost 3 dB (with the SW lens, showing proof-of-concept), and with the first sidelobe level reduced by almost 2 dB. Moreover, this caused the aperture efficiency, when compared to the non-lens LWA design, to be doubled. Also, the scanning behavior was not altered suggesting the lens does not significantly change the LW phase constant, which is responsible for radiation (e.g., the main beam angular position). In addition, the polar plots reported in Fig. 15 show general agreement with simulations for the LWA in Fig. 13.

As discussed for the near-field measurements of the SW lenses, a PICO probe positioner was retrofitted with an integrated circuit probing station (see Fig. 7), and a similar (but more compact) setup was implemented on the far-field antenna positioner for radiation studies and experimentation in the anechoic chamber. In addition, microwave absorber covered unwanted ceramic and metallic features of the setup. Regardless, such a practical testing platform can inadvertently cause unwanted reflections and scattering, potentially leading to higher than desired sidelobe levels at some frequencies and angular positions, which are observed in Fig. 15 for example; i.e., the measured sidelobe levels are more than 3 dB higher when compared to the simulations.

Overall, considering the practical challenges of this setup, the measurements are considered to be consistent with the simulations in terms of the main beam position as well as pattern shape and the relative gain values demonstrating proof-of-concept. On the other hand, should it be desired and in future work, a different measurement setup could be explored or additional techniques to reduce the sidelobe levels could be introduced. For instance, tapering

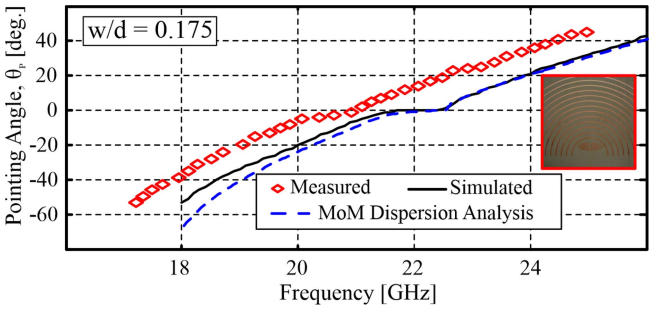

FIGURE 16. Simulations, measurements and theoretical MoM analysis for the pointing angle versus frequency for the LWA using a directive SWL at the origin. A downward shift in the measured pointing angle is observed and this is likely related to a slightly higher dielectric constant than expected, but still within the tolerance stated by the PCB manufacturer. Similar findings have been reported in [25] for the employed GDS.

within the radiating aperture could be implemented (see, e.g., [25], [26], [27]) when designing these types of LWA structures.

A dispersion analysis was also performed to characterize the leaky mode supported by the corresponding linearized version of the annular MSG presented in Fig. 13, having width and periodicity $w/d = 1.1$ mm/6.3 mm $= 0.175$. The results are reported in Fig. 16 and employ the Method of Moments (MoM). For further details see [19] and [24], and references therein. This figure also provides a comparison among the expected theoretical pointing angle for the main beam (given by LW theory, i.e., $\theta_p \approx \sin^{-1}(\beta_{LW}/k_0)$) with the one achieved through experiments. The simulations and measurements also show good agreement with conventional beam scanning from -60° to 42°. The downward frequency shift for the measured pointing angle is likely related to a practical tolerance in the relative dielectric constant of the employed Rogers 6010 substrate, which was similarly reported in [19], [23], [25] and other works referenced therein.

By utilizing the directive SWL and the planar SW lens configuration for diverging SWs, and by the addition of an appropriate half-annular metallic strip aperture, cylindrical leaky waves (CLWs) can be excited realizing far-field beam scanning as a function of frequency. With such an enlarged effective aperture, when compared to the same structure with no lens, directive pencil beam patterns can be generated in the far-field and with reduced cross-polarization levels (see Fig. 13). It should also be noted that a broadside null was measured at about 21 GHz suggesting stop band behavior. In addition, the beam scanned from backward endfire to broadside for $f < 20.3$ GHz and continued beam scanning for $f > 21$ GHz (see Fig. 16).

While the antenna efficiency and gain have been shown to be improved, the printed SW lenses take additional space and require careful positioning when integrating with the LWA and SWL. Basically, the added TPMG elements, which define the printed SW lenses, do not significantly contribute to the far-field (and therefore do not increase the total number of radiating elements defining the equivalent aperture of the antenna). Also, as shown and without such lenses, the LWA would suffer from a cylindrical SWL profile or a non-uniform wavefront, and this would likely not present improved efficiency and gain for more standard MSG-based LWAs. Also, should higher aperture efficiencies be required, additional tapering techniques could be adopted [25], [26], [27], or more optimal MSG positioning with respect to the antenna source [28], and more compact implementations (see [24], [29] and references therein) which exploit multi-layering for example. Regardless, the proposed SW lens solution in this paper can be considered advantageous due to its single-layer printed implementation and more classic MSG configuration which exploits well known LW radiation principles.

V. CONCLUSION

Planar SW lenses, one converging and one diverging, have been designed and tested in this work to improve the radiation performance of two conventional planar LWAs: a linear MSG structure and an half-annular bull-eye LWA, whilst considering a SWL feeder.

A ray-tracing technique has been applied to determine the focal point position and size of the metasurface lens, and a Yagi-Uda-like directive SWL has been co-designed with the lenses to properly tailor the propagation of the efficiently excited TM_0 SW mode. The proposed planar lenses also showed the possibility of correcting the SW phase front to generate a more stable plane-wave-like response, whilst the diverging lens modified the bound TM SW profile to a more spherical-like-wave when considering magnitude. This increased the relative power distribution across the top air-dielectric interface.

The lens structures were also integrated into classical LWAs. The lens improved the realize gain by about 3 dB_i and produced a single maximum in comparison to the non-lens design. The half-annular LWA also offered suppressed side lobe levels and reduced cross-polarization levels. More importantly, both designs do not alter the LW scanning behavior and this has been tested by means of a full-wave analysis, verifying that the far-field scanning characteristics are not affected by the presence of the lenses. Future work can include up-scaling to higher microwave and millimeter-wave frequencies of operation. The proposed lenses and LWA designs are applicable to practical scenarios which require high gain as well as low-cost and planar implementation, such as radar and communication systems.

REFERENCES

[1] X. Liu, Z. Yan, E. Wang, T. Zhang, and F. Fan, "Magnetoelectric dipole-fed fabry–perot antenna with wideband RCS reduction based on multilayer metasurface," *IEEE Antennas Wireless Propag. Lett.*, vol. 20, pp. 1342–1346, 2021.

[2] S. Vellucci et al., "On the use of nonlinear metasurfaces for circumventing fundamental limits of mantle cloaking for antennas," *IEEE Trans. Antennas Propag.*, vol. 69, no. 8, pp. 5048–5053, Aug. 2021.

[3] S. Liu, D. Yang, Y. Chen, K. Sun, X. Zhang, and Y. Xiang, "Low-profile broadband metasurface antenna under multimode resonance," *IEEE Antennas Wireless Propag. Lett.*, vol. 20, pp. 1696–1700, 2021.

[4] P.-S. Kildal, "Artificially soft and hard surfaces in electromagnetics," *IEEE Trans. Antennas Propag.*, vol. 38, no. 10, pp. 1537–1544, Oct. 1990.
[5] M. Li, S.-Q. Xiao, and D. F. Sievenpiper, "Polarization-insensitive holographic surfaces with broadside radiation," *IEEE Trans. Antennas Propag.*, vol. 64, no. 12, pp. 5272–5280, Dec. 2016.
[6] L. Matekovits, G. C. V. Colome, and M. Orefice, "Controlling the bandlimits of TE-surface wave propagation along a modulated microstrip-line-based high impedance surface," *IEEE Trans. Antennas Propag.*, vol. 56, no. 8, pp. 2555–2562, Aug. 2008.
[7] N. M. Mohamed-Hicho, E. Antonino-Daviu, M. Cabedo-Fabrés, and M. Ferrando-Bataller, "A novel low-profile high-gain UHF antenna using high-impedance surfaces," *IEEE Antennas Wireless Propag. Lett.*, vol. 14, pp. 1014–1017, 2015.
[8] X. Chen, L. Li, C. H. Liang, Z. J. Su, and C. Zhu, "Dual-band high impedance surface with mushroom-type cells loaded by symmetric meandered slots," *IEEE Trans. Antennas Propag.*, vol. 60, no. 10, pp. 4677–4687, Oct. 2012.
[9] D. S. Chandu and S. S. Karthikeyan, "A miniaturized broadband high-impedance surface with flexible circular polarization sense," *IEEE Trans. Antennas Propag.*, vol. 67, no. 4, pp. 2819–2824, Apr. 2019.
[10] Q. Lv, Y. Tang, B. Zhang, L. Yin, C. Jin, and R. Mittra, "Dual-band diffusive metasurface-based reflector with low out-of-band backscattering," *IEEE Access*, vol. 8, pp. 217196–217203, 2020.
[11] W. Li, Y. M. Wang, Y. Hei, B. Li, and X. Shi, "A compact low-profile reconfigurable metasurface antenna with polarization and pattern diversities," *IEEE Antennas Wireless Propag. Lett.*, vol. 20, pp. 1170–1174, 2021.
[12] V. G. Ataloglou, M. Chen, M. Kim, and G. V. Eleftheriades, "Microwave huygens' metasurfaces: Fundamentals and applications," *IEEE J. Microw.*, vol. 1, no. 1, pp. 374–388, Jan. 2021.
[13] C. Pfeiffer and A. Grbic, "Metamaterial huygens' surfaces: Tailoring wave fronts with reflectionless sheets," *Phys. Rev. Lett.*, vol. 110, May 2013, Art. no. 197401.
[14] J. Brown, *Lens Antennas, in Antenna Theory, Part 2*. New York, NY, USA: McGraw-Hill, 1969.
[15] D. G. Dalgoutte and C. D. W. Wilkinson, "Thin grating couplers for integrated optics: An experimental and theoretical study," *Appl. Opt.*, vol. 14, no. 12, pp. 2983–2998, Dec. 1975.
[16] S. T. Peng and T. Tamir, "TM-mode perturbation analysis of dielectric gratings," *Appl. Phys.*, vol. 7, pp. 35–38, May 1975.
[17] W. E. Cock, "Metallic delay lenses," *Bell Syst. Tech. J.*, vol. 27, no. 1, pp. 58–82, Jan. 1948.
[18] S. K. Podilchak, A. P. Freundorfer, and Y. M. M. Antar, "Surface-wave launchers for beam steering and application to planar leaky-wave antennas," *IEEE Trans. Antennas Propag.*, vol. 57, no. 2, pp. 355–363, Feb. 2009.
[19] S. Podilchak, "Planar leaky-wave antennas and microwave circuits by practical surface wave launching," Ph.D. dissertation, Dept. Electr. Comput. Eng., Queen's Univ., Kingston, ON, Canada, 2013.
[20] A. F. Perkons, Y. Qian, and T. Itoh, "TM surface-wave power combining by a planar active-lens amplifier," *IEEE Trans. Microw. Theory Tech.*, vol. 46, no. 6, pp. 775–783, Jun. 1998.
[21] M. Ettorre, S. Bruni, G. Gerini, A. Neto, N. Llombart, and S. Maci, "Sector PCS-EBG antenna for low-cost high-directivity applications," *IEEE Antennas Wireless Propag. Lett.*, vol. 6, pp. 537–539, 2007.
[22] S. K. Podilchak, A. P. Freundorfer, and Y. M. M. Antar, "Planar leaky-wave antenna designs offering conical-sector beam scanning and broadside radiation using surface-wave launchers," *IEEE Antennas Wireless Propag. Lett.*, vol. 7, pp. 155–158, 2008.
[23] S. K. Podilchak, P. Baccarelli, P. Burghignoli, A. P. Freundorfer, and Y. M. M. Antar, "Analysis and design of annular microstrip-based planar periodic leaky-wave antennas," *IEEE Trans. Antennas Propag.*, vol. 62, no. 6, pp. 2978–2991, Jun. 2014.
[24] D. Comite et al., "Analysis and design of a compact leaky-wave antenna for wide-band broadside radiation," *Nat. Sci. Rep.*, vol. 8, no. 1, pp. 1–14, 2018.
[25] M. V. Kuznetcov, V. G.-G. Buendía, Z. Shafiq, L. Matekovits, D. E. Anagnostou, and S. K. Podilchak, "Printed leaky-wave antenna with aperture control using width-modulated microstrip lines and TM surface-wave feeding by SIW technology," *IEEE Antennas Wireless Propag. Lett.*, vol. 18, pp. 1809–1813, 2019.
[26] J.-H. Lu, J.-H. Huang, C. F. Jou, and L.-K. Wu, "Side lobe suppression of a short leaky-wave antenna by phase constant tapering: Analysis and design," *IEEE Trans. Antennas Propag.*, vol. 63, no. 8, pp. 3774–3779, Aug. 2015.
[27] K. Wang, Y. Xiao, Y. Li, Z. Liang, S. Y. Zheng, and Y. Long, "A tapered continuous-element leaky-wave antenna with pure radiation pattern," *IEEE Antennas Wireless Propag. Lett.*, vol. 20, no. 9, pp. 1804–1808, Sep. 2021.
[28] S. K. Podilchak, P. Baccarelli, P. Burghignoli, A. P. Freundorfer, and Y. M. M. Antar, "Optimization of a planar "bull-eye" leaky-wave antenna fed by a printed surface-wave source," *IEEE Antennas Wireless Propag. Lett.*, vol. 12, pp. 665–669, 2013.
[29] D. Comite et al., "A dual-layer planar leaky-wave antenna designed for linear scanning through broadside," *IEEE Antennas Wireless Propag. Lett.*, vol. 16, pp. 1106–1110, 2017.

MAKSIM V. KUZNETCOV (Member, IEEE) was born in Kopeysk, Russia, in 1993. He received the M.Eng. degree in electrical and electronic engineering from Heriot-Watt University, Edinburgh, U.K., in 2019, and the Ph.D. degree from Heriot-Watt University, Edinburgh, and the University of Edinburgh, Edinburgh, in 2022.

His research interests include the analysis and design of leaky-wave antennas, duplex and polarization-diverse antenna systems, active circuits, and other microwave and antenna technologies. He received the Engineering and Physical Sciences Thesis Prize.

DAVIDE COMITE (Senior Member, IEEE) received the master's degree (cum laude) in telecommunications engineering and the Ph.D. degree in electromagnetics and mathematical models for engineering from Sapienza University Rome, Rome, Italy, in 2011 and 2015, respectively. He is currently a Tenure Track Assistant Professor with Sapienza University Rome. He was a visiting Ph.D. student with the Institute of Electronics and Telecommunications of Rennes, University of Rennes 1, France, in 2014, and a Postdoctoral Researcher with the Center of Advanced Communications, Villanova University, Villanova, PA, USA, in 2015. He has been leading the Global Navigation Satellite System Reflectometry (GNSS-R) Modeling Working Group of the GRSS MIRS Technical Committee since January 2021. Since November 2020, he is one of the officers of the Young Professional Affinity Group of the IEEE Italian Chapter. His scientific interests involve Earth observation, remote sensing, the study of the scattering from natural surfaces, the GNSS-R over land, and radar altimetry for biomass monitoring. He is also interested in the study and design of microwaves and millimeter-waves antennas, antenna arrays, leaky waves, leaky-wave antennas, as well as in the generation of nondiffracting waves and pulses. He has been a recipient of awards at both national and international conferences. In 2019, 2020, and 2021, the IEEE Antennas and Propagation Society recognized him as an Outstanding Reviewer for the IEEE TRANSACTION ON ANTENNAS AND PROPAGATION. In 2020, he was awarded as the Best Reviewer for the IEEE JOURNAL OF SELECTED TOPICS IN APPLIED EARTH OBSERVATION AND REMOTE SENSING. Since March 2022, he has been the Chair of the ECAP Working Group of EuRAAP. He is an Associate Editor of the IEEE JOURNAL OF SELECTED TOPICS IN APPLIED EARTH OBSERVATION AND REMOTE SENSING, the *EurAAP Journal Reviews of Electromagnetics*, the *IET Journal of Engineering*, the *IET Microwaves, Antennas and Propagation* by the Institution of Engineering and Technology, and IEEE ACCESS. He is an URSI Senior Member.

SYMON K. PODILCHAK (Member, IEEE) received the B.A.Sc. degree in engineering science from the University of Toronto, Toronto, ON, Canada, in 2005, and the M.A.Sc. and Ph.D. degrees in electrical engineering from Queen's University, Kingston, ON, Canada, in 2008 and 2013, respectively.

From 2013 to 2015, he was an Assistant Professor with Queen's University. In 2015, he joined Heriot-Watt University, Edinburgh, U.K., as an Assistant Professor, and became an Associate Professor in 2017. He is currently a Senior Lecturer with the School of Engineering, The University of Edinburgh, Edinburgh, U.K. He has had industrial experience as a computer programmer, and has designed 24 and 77 GHz automotive radar systems with Samsung and Magna Electronics. His recent industry experiences also include the design of high frequency surface-wave radar systems, professional software design and implementation for measurements in anechoic chambers for the Canadian Department of National Defense and the SLOWPOKE Nuclear Reactor Facility. He has also designed compact antennas for wideband military communications, highly compact circularly polarized antennas for CubeSats with COM DEV International (currently Honeywell) and The European Space Agency, and new wireless power transmission systems for Samsung. His research interests include surface waves, leaky-wave antennas, metasurfaces, UWB antennas, phased array antenna systems, and RF integrated circuits.

Dr. Podilchak and his students have been the recipient of many best paper awards and scholarships, most notably Research Fellowships from the IEEE Antennas and Propagation Society (AP-S), IEEE Microwave Theory and Techniques Society (MTT-S), European Microwave Association, and six Young Scientist Awards from the International Union of Radio Science. He was a recipient of a Fellowship from the Natural Sciences and Engineering Research Council of Canada. In 2011, 2013, 2020, and 2021, he and his students were the recipient of Student Paper Awards at the IEEE International Symposium on Antennas and Propagation. In 2012, the Best Paper Prize for Antenna Design at the European Conference on Antennas and Propagation for his work on CubeSat antennas, and in 2016, European Microwave Prize for his research on surface waves and leaky-wave antennas. In 2017 and 2019, he was bestowed a Visiting Professorship Award at Sapienza University, Rome, Italy, and from 2016 to 2019, his research was supported by a H2020 Marie Sklodowska-Curie European Research Fellowship. In 2021, he was also the recipient of the COVID-19 Above and Beyond Medal for leading research on remote microwave sterilization of the coronavirus. He was also the Founder and the First Chairman of the IEEE AP-S and IEEE MTT-S Joint Chapters in Canada and Scotland, in 2014 and 2019, respectively. In recognition of these services, he was presented with an Outstanding Volunteer Award from IEEE MTT-S and AP-S in 2015, and in 2020 and 2021, respectively, IEEE recognized this Scotland Chapter for its activities and it was awarded the winner of the Outstanding Chapter Award hosted by these two IEEE Societies. He was also the recipient of the Outstanding Dissertation Award for his Ph.D. He was a Lecturer with the European School of Antennas and an Associate Editor for the *IET Electronics Letters*. He was recognized as an outstanding Reviewer of the IEEE TRANSACTIONS ON ANTENNAS AND PROPAGATION in 2014 and 2020. He was also a Guest Associate Editor for the IEEE OPEN JOURNAL OF ANTENNAS AND PROPAGATION and IEEE ANTENNAS AND WIRELESS PROPAGATION LETTERS. He is currently an Associate Editor of IEEE TRANSACTIONS ON ANTENNAS AND PROPAGATION. He is also a Registered Professional Engineer.

ALOIS P. FREUNDORFER (Life Senior Member, IEEE) received the B.A.Sc., M.A.Sc., and Ph.D. degrees from the University of Toronto, Toronto, ON, Canada, in 1981, 1983, and 1989, respectively. In 1990, he joined the Department of Electrical Engineering, Queen's University, Kingston, ON, Canada. Since 1990, he has been involved in the nonlinear optics of organic crystals, coherent optical network analysis, and microwave integrated circuits. He was involved in high-speed IC design for use in lightwave systems with bit rates in excess of 40 Gb/s and in millimeter wave integrated circuits used in wireless communications. His current research interests include growing 3-D low-temperature ceramics on ICs and printed circuit boards with applications to sensors and low power tunable circuits.

YAHIA M. M. ANTAR (Life Fellow, IEEE) received the B.Sc. degree (Hons.) in electrical engineering from Alexandria University, Alexandria, Egypt, in 1966, and the M.Sc. and Ph.D. degrees in electrical engineering from the University of Manitoba, Winnipeg, MB, Canada, in 1971 and 1975, respectively. In May 1979, he joined the Division of Electrical Engineering, National Research Council of Canada, Ottawa, ON, Canada. In November 1987, he joined the Department of Electrical and Computer Engineering, Royal Military College of Canada, Kingston, ON, Canada, where he has been a Professor since 1990. He has authored or coauthored over 200 journal articles, several books, and chapters in books, over 450 refereed conference papers and holds several patents. He was awarded the Royal Military College of Canada "Excellence in Research" Prize in 2003 and the RMCC Class of 1965 Teaching Excellence Award in 2012. In October 2012, he received the Queen's Diamond Jubilee Medal from the Governor-General of Canada in recognition of his contribution to Canada. He was a recipient of the 2014 IEEE Canada RA Fessenden Silver Medal for Ground Breaking Contributions to Electromagnetics and Communications and the 2015 IEEE Canada J. M. Ham Outstanding Engineering Education Award. In May 2015, he received the Royal Military College of Canada Cowan Prize for excellence in research. He was also a recipient of the IEEEAP-S of the Chen-To-Tai Distinguished Educator Award in 2017. He has supervised and co-supervised over 90 Ph.D. and M.Sc. theses with the Royal Military College of Canada and Queen's University, Kingston, several of which have received the Governor-General of Canada Gold Medal Award, the Outstanding Ph.D. Thesis of the Division of Applied Science, as well as many best paper awards in major international symposia. He served as the Chair for Canadian National Commission, International Union of Radio Science (URSI) from 1999 to 2008 and Commission B from 1993 to 1999, and has a cross-appointment at Queen's University. In May 2002, he was awarded the Tier 1 Canada Research Chair in electromagnetic engineering which has been renewed in 2016. He was elected by the URSI to the Board as the Vice President in August 2008 and 2014, and to the IEEE Antennas and Propagation (AP-S) AdCom. In 2019, he was elected as the 2020 President-Elect for IEEE AP-S, and served as its President in 2021. He has served as an Associate Editor for many IEEE and IET journals and an IEEE-APS Distinguished Lecturer. He has chaired several national and international conferences, and has given plenary talks at many conferences. He was appointed as a member of the Canadian Defence Advisory Board of the Canadian Department of National Defence in January 2011. He is a Fellow of the Engineering Institute of Canada and the Electromagnetic Academy. He is also a URSI Fellow. In 1977, he held a Government of Canada Visiting Fellowship at the Communications Research Center, Ottawa.

Open Access funding provided by 'Università degli Studi di Roma "La Sapienza" 2' within the CRUI CARE Agreement